2001

Some Perspectives on Recent In Situ Air Temperature Observations: Modeling the Microclimate inside the Radiation Shields*

X. Lin

Kenneth Hubbard

Elizabeth A. Walter-Shea

James Brandle

G.E. Meyer

Some Perspectives on Recent In Situ Air Temperature Observations: Modeling the Microclimate inside the Radiation Shields*

X. LIN, K. G. HUBBARD, E. A. WALTER-SHEA, AND J. R. BRANDLE

School of Natural Resource Sciences, University of Nebraska, Lincoln, Lincoln, Nebraska

G. E. MEYER

Biological Systems Engineering Department, University of Nebraska, Lincoln, Lincoln, Nebraska

(Manuscript received 8 May 2000, in final form 12 December 2000)

ABSTRACT

Air temperature measurement has inherent biases associated with the particular radiation shield and sensor deployed. The replacement of the Cotton Region Shelter (CRS) with the Maximum–Minimum Temperature System (MMTS) and the introduction of Automated Surface Observing System (ASOS) air temperature observing systems during the NWS modernization introduced bias shifts in federal networks that required quantification. In rapidly developing nonfederal networks, the Gill shield temperature systems are widely used. All of these systems house an air temperature sensor in a radiation shield to prevent radiation loading on the sensors; a side effect is that the air temperature entering a shield is modified by interior solar radiation, infrared radiation, airspeed, and heat conduction to or from the sensor so that the shield forms its own interior microclimate. The objectives of this study are to develop an energy balance model to evaluate the microclimate inside the ASOS, MMTS, Gill, and CRS shields, including the interior solar radiation, infrared radiation, and airspeed effects on air (sensor) temperature under day and night conditions. For all radiation shields, the model air temperature for shield effects was in good agreement between shields while the uncorrected ''normal operating'' temperatures were more variable from shield to shield. The solar radiation loading ratio was dramatically increased with a corresponding increase in the solar elevation angle for all shields except the ASOS shield, and are ranked as Gill $>$ MMTS $\approx$ CRS $>$ ASOS. The daytime infrared radiation effects on air temperature were ranked as ASOS $>$ Gill $>$ MMTS $>$ CRS, but the nighttime infrared radiation effects were not so large and were uniformly distributed among negative and positive effects on air temperatures. For the nonaspirated radiation shields (MMTS, Gill, and CRS), increasing ambient wind speed improved the accuracy of air temperatures, but it was impossible to reach the accuracy claimed by manufacturers when the in situ measurements were taken under lower ambient wind speed ($<4 \sim 5$ m s^{-1}).

1. Introduction

The goal in weather monitoring is to accurately measure and record standard meteorological variables like air temperature, precipitation, air humidity, solar radiation, wind speed and direction, and soil temperature. Air temperature is considered one of the most important variables in efforts to recognize and evaluate the extent of human impacts on climate from local to global scales. The instrumented climate record holds information on the spatial distribution and secular trends in temperature over many areas of the world (Karl et al. 1989). Unfortunately, inhomogeneities in the air temperature records may mask the signal of climate change. For example, with the advances in instrumentation and measurement technology, significant changes in temperature measurements took place. Such instrumentation changes introduce systematic biases and are therefore a major factor in the uncertainty in observed temperature trends. How can we quantify the degree of observed global climate change until we know the effects of instrumentation upgrades on the accuracy or representativeness of weather station measurements? Climatologists are struggling to answer such questions, not only to satisfy scientific curiosity but also to aid policy makers and the public at large.

Several major technological changes in monitoring temperature have occurred during the past few decades. A new smaller radiation shield called the Gill radiation shield (Gill 1979, 1983) was introduced in automated weather station networks. In the mid- and late-1980s, the widely used air temperature radiation shield called

* Nebraska Agricultural Experiment Station Journal Number 13008.

Corresponding author address: Dr. Kenneth G. Hubbard, 242 L. W. Chase Hall, University of Nebraska, Lincoln, Lincoln, NE 68583-0728.
E-mail: khubbard1@unl.edu

the Cotton Region Shelter (CRS) was gradually replaced by the Maximum and Minimum Temperature System (MMTS) in the cooperative weather station network. In the 1990s the Automated Surface Observing System (ASOS) replaced conventional observations at National Weather Service (NWS) and Federal Aviation Administration stations that report hourly observations. There are fundamental differences among the liquid-in-glass (LIG) thermometer used in CRS, the thermistor sensor used in the MMTS, an HMP35C temperature sensor (Vaisala Inc., Finland) used in the Gill shield, and the platinum resistance thermometer (PRT) used in the ASOS. Therefore, it is highly likely that systematic biases are present in the record because of influences of shields and characteristics of sensors. A shield affects the heating or cooling from solar radiation (SR, infrared radiation IR), and ventilation. Sensors respond differently to forcing functions inside the shield such as heat conduction through the sensor's attachment points, infrared radiation emitted by the sensor, and convection heat exchange with the air surrounding the sensor. Although the question of which system is the most accurate is interesting, it now becomes secondary to the goal of understanding and modeling the biases so that transfer functions can be developed and homogeneous historical datasets produced.

Numerous studies have investigated both shield performance and errors in air temperature caused by shields, including both field and wind tunnel tests (MacHattie 1965; Fuchs and Tanner 1965; Sterling Research & Development Center 1973; McTaggart-Cowan and McKay 1976; McKay and McTaggart-Cowan 1977; Tanner et al. 1996). The main finding from these studies is that air temperature errors caused by a radiation shield could range from $-0.5°$ to 2.5°C. Gill (1983) conducted low-speed wind tunnel tests of several radiation shields under high radiation from lamps that simulated the sun. Gill found that certain shields could have 2 to 4 times the radiation heating error as others. There was a 6°C radiation heating error for the Gill shield at low wind speeds, which for those conditions was the minimum error among several shields offered commercially at the time. Brock et al. (1995a,b) and Richardson and Brock (1995) proposed an optimal radiation shield design and sensor design that would minimize both direct and indirect radiation loadings and maximize the airflow.

Many researchers conducted intercomparisons between new and old temperature systems. Wendland and Armstrong (1993) performed a comparison between LIG maximum temperature and MMTS maximum temperature showing as much as a 0.6°C difference. Bradley and Bradley (1995) reported that the average monthly differences between the CRS and MMTS ranged from 0.6° to 1.3°C and 0.0° to 1.3°C for daily maximum and minimum temperatures, respectively. This change, from LIG inside the CRS to a thermistor inside the MMTS, may have affected the data continuity of the nation's long-term climate datasets (Doesken et al. 1995). Based on thousands of comparisons of monthly mean temperatures from stations with and without MMTS, Quayle et al. (1991) found that the MMTS system on average produces maximum temperatures about 0.4°C lower and minimum temperatures about 0.3°C higher than the CRS system.

ASOS did not always have the same temperature monitoring system from site to site or year to year, owing to the fact that both the HO-83 ASOS (first deployment) and the 1088 ASOS were utilized. Unfortunately, there are differences in temperature readings between the two versions of ASOS. McKee et al. (1993) reported systematic temperature differences between the 1088 ASOS and its predecessor (an earlier version of HO-83) of -0.79°C (-1.43°F) for daily maximum and -0.81°C (-1.46°F) for daily minimum temperature on average for 16 stations and 3 months of data. Bradley (1994) compared the daily maximum temperature difference between the R. M. Young air temperature system and the HO-83 ASOS temperature for a typical August in 1992. Differences were surprisingly high ranging from $-0.3°$ to 2.9°C. Much of the error was attributed to the HO-83 ASOS system since the R. M. Young temperature system is widely accepted by researchers for obtaining reference temperature observations. Gall et al. (1992) analyzed temperature data from 1986 to 1990 in Tucson, Arizona. They questioned whether the recent maximum temperature anomalies in Tucson were real or the result of an instrument problem. The study concluded that the increase in anomalies was due to changes in the temperature observing system associated with ASOS upgrades. Kessler et al. (1993) analyzed the daily maximum temperature bias introduced by the replacement of an HO-63 Hygrothermograph with an HO-83 instrument at Albany, New York. His findings were similar to Gall et al. (1992) in Tucson. The HO-83 maximum temperature readings were about $+1°$ to $+3$°C higher on sunny, light wind days. The research of both Kessler et al. (1993) and Gall et al. (1992) illustrates the need to account for shield/sensor bias prior to analysis of operational NWS temperature data and determination of short-term temperature trends. Other researchers (Robinson 1990; Canfield and McNitt 1991; Meyer and Hubbard 1992; Croft and Robinson 1993; Blackburn 1993; Easterling et al. 1993; Guttman and Baker 1996; Andresen and Numberger 1997), in various ways, pointed out the climate data discontinuities and trends or changes in variability resulting from changes of temperature measuring systems and site locations.

The specific objective of the present study is to develop a prototype system to study the effect of radiation shields on the measurement of air temperature. The aim is to understand how each air temperature radiation shield influences the microenvironment of the corresponding temperature sensor. To do this, the extent to which the shields modify radiation and control ventilation of sensors (natural ventilation inside the MMTS, Gill, and CRS shields or forced air movement inside the

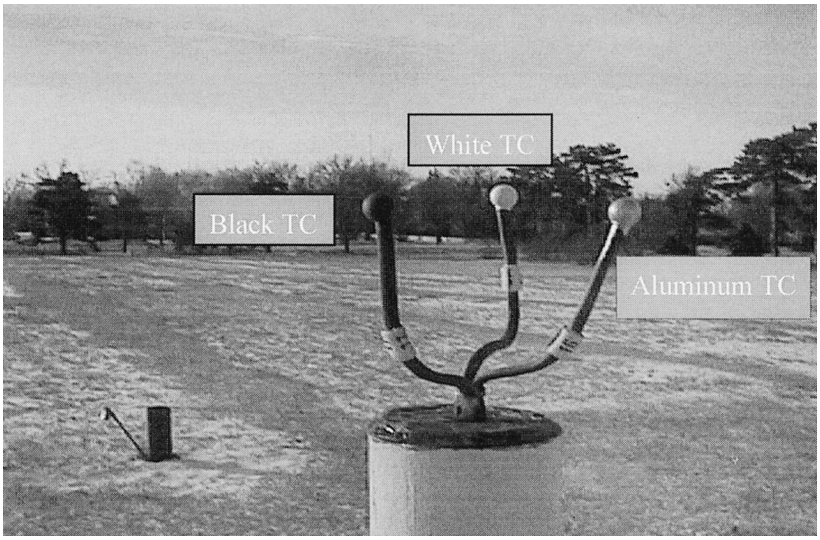

FIG. 1. Close-up of the prototype EBTC exposed without radiation shield. Exposed spherical painted thermocouples are 5.8 mm in diameter.

ASOS) must be determined. To accomplish this, the following aspects were investigated:

1) the ''true'' air temperature obtained from an energy balance thermocouple (EBTC),
2) interior SR and IR effects on the sensor temperature under day and night conditions, and
3) normal operating (NP) air temperature errors related to microclimate during the daytime and nighttime.

2. Materials and methods

a. EBTC model

Multithermistor radiosonde techniques (Luers 1989, 1992; Luers and Eskridge 1995; Schmidlin et al. 1995) were successfully developed for temperature corrections to Radiosonde data. Similarly, Wylie and Lalas (1992) used three PRT sensors to construct a system to evaluate the World Meteorological Organization reference psychrometer. The main objective of this technique is to increase the measured accuracy of air temperature by removing the radiation (solar and infrared) and convection heat transfer effects on air temperature measurements. An EBTC system was used in the present study to monitor the interior microclimate of air temperature radiation shields. The EBTC system (Fig. 1) provides a separate temperature signal from each of three EBTC sensors. Each EBTC sensor consists of a thermocouple [precision fine-wire type E thermocouple (OMEGA Engineering, Inc. 1995)] embedded in a brass sphere (4.76 mm in diameter) with thermcoat cement. The surface of each brass sphere was painted aluminum, black, or white with a thickness of 0.5 mm for each sensor using enamel paint (RUST-OLEUM Co.). Thus each sphere was 5.76 mm in diameter. The aluminum, black, and white coatings each have different absorption and emission properties and thus reach different equilibrium temperatures for given SR and IR conditions. An energy balance equation can be written for each of the EBTC sensors. The EBTC model consists of the following three equations for the aluminum, black, and white EBTC sensors, respectively:

$$mc\frac{dT_a}{dt} = \alpha_a \mathrm{SR} + \varepsilon_a \mathrm{IR} - \sigma\varepsilon_a A T_a^4 - AH(T_a - T_{\mathrm{air}}) + A_{\mathrm{wi}} k_{\mathrm{wi}} \frac{dT_{\mathrm{wi}}}{dl_a} + i_a^2 R_a, \quad (1)$$

$$mc\frac{dT_b}{dt} = \alpha_b \mathrm{SR} + \varepsilon_b \mathrm{IR} - \sigma\varepsilon_b A T_b^4 - AH(T_b - T_{\mathrm{air}}) + A_{\mathrm{wi}} k_{\mathrm{wi}} \frac{dT_{\mathrm{wi}}}{dl_b} + i_b^2 R_b, \quad \text{and} \quad (2)$$

$$mc\frac{dT_w}{dt} = \alpha_w \mathrm{SR} + \varepsilon_w \mathrm{IR} - \sigma\varepsilon_w A T_w^4 - AH(T_w - T_{\mathrm{air}}) + A_{\mathrm{wi}} k_{\mathrm{wi}} \frac{dT_{\mathrm{wi}}}{dl_w} + i_w^2 R_w, \quad (3)$$

where

m = mass of the EBTC sensor (Kg),
c = specific heat capacity of the EBTC sensor (J Kg^{-1} K^{-1});
t = time (s),
T_a, T_b, T_w = temperature of aluminum, black, and white EBTC sensors (K);
α_a, α_b, α_w = solar absorptivities of aluminum, black, and white EBTC sensors;
ε_a, ε_b, ε_w = infrared emissivities of aluminum, black, and white EBTC sensors;

TABLE 1. Solar absorptivity and infrared emissivity of the thermocouple coatings.

	Solar absorptivity (α)	Infrared emissivity (ϵ)
Aluminum thermocouple	0.31	0.55
Black thermocouple	0.94	0.93
White thermocouple	0.15	0.95

SR = solar radiation loading on the EBTC sensor (W);
IR = infrared radiation loading on the EBTC sensor (W);
A = surface area of the EBTC sensor (m^2),
H = convection heat transfer coefficient (W m^{-2} K^{-1});
T_{air} = air temperature (K),
σ = Stefan–Boltzmann constant (5.67×10^{-8} W m^{-2} K^{-4});
A_{wl} = cross-section area of EBTC sensor lead wires (m^2);
k_{wl} = thermal conductivity of the lead wires (W m^{-1} K^{-1});
T_{wl} = temperature of EBTC sensor lead wires (°C);
l_a, l_b, l_w = length of the lead wires (m);
i_a, i_b, i_w = electrical current through EBTC sensor junction (A); and
R_a, R_b, R_w = resistance of EBTC sensor with brass ball junction (Ω).

The EBTC model contains all significant energy (or heat) transfer terms known to affect each spherical EBTC sensor. The EBTC sensors are all exposed to the same environment; therefore, the unknowns T_{air}, SR, and IR are obtained by simultaneous solution of these three equations. The interior SR and IR include the direct, reflected, and scattered radiation entering from all view directions. To solve Eqs. (1)–(3) for the air temperature T_{air}, SR, and IR, the constants and other parameters in Eqs. (1)–(3) must first be identified.

b. Determination of EBTC model parameters

The EBTC model assumes that the mass, dimensions, and orientations of all EBTC sensors are identical. The mass of each EBTC sensor was 0.72 g and the surface area was 1.0×10^{-4} m^2. The specific heat capacity (c) of each EBTC sensor was determined to be 400 J Kg^{-1} K^{-1} for all Eqs. [(1)–(3)]. The net energy terms on the left side of Eqs. (1)–(3) can be calculated using real-time temperature readings from each EBTC sensor.

The spectral directional emissivity of a surface (ε_{sen}) in a given direction is equal to its spectral absorptivity (α_{sen}) for flux incident from the same direction (Dewitt and Nutter 1989). Thus,

$$\varepsilon_{sen}(\lambda, \theta', \varphi', T_{sen}) = \alpha_{sen}(\lambda, \theta, \varphi, T_{sen}), \quad (4)$$

where (θ', φ') and (θ, φ) refer to zenith and azimuth of the same path but opposite direction, λ refers to the wavelength, and T_{sen} refers to the sensor surface temperature. The absorptivity was measured spectrally for each coating over wavelengths from 0.35–1.85 μm using a spectrometer made by Analytical Spectral Devices, Inc. and the infrared emissivity was measured using an infrared emissivity device (Lin 1999) for wavelengths from 8–14 μm (Table 1).

The convection heat transfer coefficient (H) was calculated from the empirical Nusselt number (Whitaker 1972) for a sphere as follows:

$$\overline{\mathrm{Nu}} = 2 + (0.4\mathrm{Re}_d^{1/2} + 0.06\mathrm{Re}_d^{2/3})\mathrm{Pr}^{0.4}\left(\frac{\mu_\infty}{\mu_w}\right)^{1/4}, \quad (5)$$

where μ_∞ and μ_w are the air dynamic viscosities (kg m^{-1} s^{-1}) at the air temperature and EBTC sensor surface temperature. The Prandtl number (Pr) is tabulated (Holman 1997) and the Reynolds number (Re_d) was calculated from

$$\mathrm{Re}_d = \frac{u_\infty d}{\upsilon}, \quad (6)$$

where u_∞ is the air speed passing across the EBTC sensor sphere (m s^{-1}); d is the diameter of the EBTC sensor sphere (m); and υ is the kinematic viscosity (m^2 s^{-1}), which can be tabulated as a function of air temperature. The determination of the u_∞ values inside each shield was calculated from ambient wind speed outside the shield (Lin et al. 2001). Therefore, the average convection heat transfer coefficient H was calculated from

$$H = \frac{k\overline{\mathrm{Nu}}}{d}, \quad (7)$$

where k is air thermal conductivity (W m^{-1} K^{-1}). From Eqs. (5)–(7) it is apparent that the convection heat transfer coefficient is a strong function of the airspeed inside a shield.

The thermal conduction through the EBTC sensor lead wire could require another heat transfer model along the EBTC sensor wire to estimate the net conduction heat transfer into the EBTC sensor. However, selection of small diameter thermocouples with low thermal conductivity (type E thermocouple), as well as good insulation, greatly attenuates the amount of heat transfer by conduction (Tarnopolsky and Seginer 1999). The EBTC sensor wire was wrapped with a foil-covered foam strip from where it joins the EBTC sensor to a length of 1.5 m. The rest of the EBTC sensor lead wire was placed in a plastic PVC conduit. Therefore, the heat transfer by conduction was assumed to be negligible. The electrical heat conduction is considered negligible compared to other energy terms in the EBTC system because of extremely small current (i_a, i_b, or i_w) and resistance (R_a, R_b, or R_w; Lin 1999).

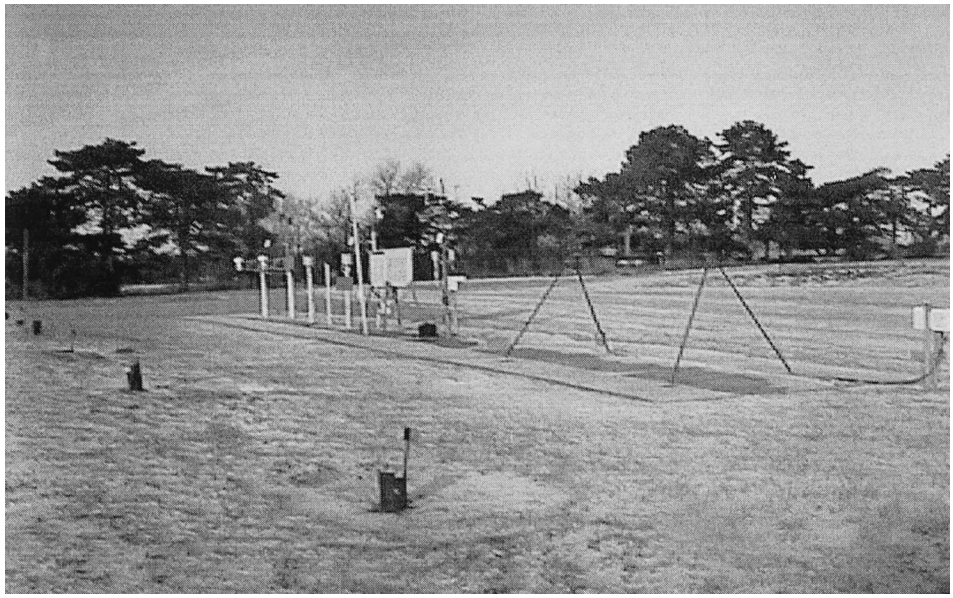

FIG. 2. From the left: pairs of ASOS and MMTS shields, a CRS, a pair of Gill shields and Met-One wind speed and direction sensors, and an A-frame for auxiliary measurements. The surface is snow-covered.

c. Experimental design and instrumentation

The experiments were conducted from early August 1997 to late August 1998 at the University of Nebraska's Horticulture Experimental Site (40°83′N, 96°67′W; altitude 383 m), located in Lincoln, Nebraska. The site has flat terrain and the surface was mowed grass; there were no physical obstructions within 25 m of the sensors. The experimental setup consisted of pairs of the ASOS, MMTS, and Gill shields and one CRS shield (Fig. 2). One shield from each pair was a control with the original ''commercial'' sensor taking measurements in a fashion similar to that during normal network operations. The second shield in each pair contained the EBTC system to monitor the interior microclimate of the shield. Because of its physical size, the CRS shelter was sufficient to hold both a commercial and an EBTC system. In the first shield of each pair, five fine-wire ''Cement-On'' thermocouples (COTC) were installed on the inner surfaces, directly in view of the EBTC sensors but without causing obstructions to airflow (the COTC thickness is 1.27 mm, 30-gage thermocouple wire). These COTCs measured the inner surface temperature (IST) directly above (top), east, south, west, and north of the EBTC. The NP air temperature sensor for the CRS is an LIG, but in order to collect data at a higher sampling rate, a thermistor sensor HMP35C was used in this study.

1) INSTRUMENTATION

All data except the ASOS temperature record were collected using three CR10 dataloggers (Campbell Scientific, Inc). The dataloggers communicated in serial mode, and one of three dataloggers was set up to communicate with a personal computer to transfer all real-time data measured at the experimental site.

Under normal ASOS operation, NWS uses a transmitter from the 1088 ASOS temperature and dewpoint sensors connected by a fiberoptic module from the sensor to the data collection package. An RS-232 communication protocol was developed for directly interrogating the 1088 ASOS using a personal computer and fiber optic modems. This allowed the ASOS data to be collected and stored in real time in a manner duplicating normal operating conditions. The MMTS temperature measurement is normally read visually by the observer from liquid-crystal display. In order to automatically record continuous readings from the MMTS sensor, the commercial thermistor for the MMTS was connected to a full bridge circuit using three high-precision resistors. The measurement accuracy of the CR10 datalogger is better than the initial MMTS readout because the signal conversion resolution and errors inside the CR10 are better than those for the initial MMTS readout. The HMP35C air temperature/humidity sensor was installed in both Gill and CRS control shields. The Met-One wind speed and wind direction sensors (Met-One Instruments) were installed nearby to monitor the airspeed and airflow direction.

The EBTC and COTC were separately interfaced by two AM25T solid-state multiplexers to the CR10 dataloggers. The AM25T multiplexer allowed connection of multiple thermocouples and provided an internal PRT at the AM25T multiplexer reference junction. For both EBTC and COTC, the type E thermocouples have low thermal conductivity and high resolution of output sig-

TABLE 2. Normal operating temperature sensor's accuracy, resolution, and range.

Shield	Element	Sensor	Accuracy (°C)	A/D resolution (bits)	Data resolution (°C)	Range (°C)
ASOS	PRT	HO-1088	±1.0	13	0.1	−50 to +50
MMTS	thermistor	MMTS	±2.0[c]	12	0.1	−35 to +50
Gill	thermistor	HMP35C	±0.4	12	0.01 or 0.001[b]	−24 to +48
CRS	thermistor	HMP35C[a]	±0.4	12	0.01 or 0.001[b]	−24 to +48

[a] Installed inside the CRS instead of the LIG thermometer.
[b] Depends on the CR10 datalogger's programming.
[c] Accuracy of thermistor interchangeability excluding the MMTS read-out errors.

nal. The EBTC and COTC extension wires were insulated using foam material with aluminum foil for a length of 2 m beginning at the AM25T multiplexer.

2) CALIBRATION AND MEASUREMENTS

The preventive and corrective maintenance procedures for the 1088 ASOS temperature/dewpoint sensor were strictly followed as prescribed in the ASOS Site Technical Manual (ASOS Program Office 1992). The 1088 ASOS was calibrated twice during the experiment period by following the calibration procedures in the manual. Although the MMTS temperature system is not usually subjected to calibration according to the operating instructions (National Weather Service 1983), the three high-precision constant resistors that constructed the full bridge measurement circuit were verified twice each year. The HMP35C temperature sensors inside the Gill shield and CRS shield were calibrated once a year using a temperature calibrator, Model D55SE (AMETEK Inc., JOFRA Instruments). The accuracy of the air temperature measurement, analog-to-digital conversion resolution, data output resolution, and range are summarized in Table 2 for the normal operation.

The EBTC and COTC were carefully calibrated with a D55SE temperature calibrator with the accuracy ±0.3°C. All EBTCs and all COTCs were simultaneously calibrated using the same AM25T multiplexers, CR10 dataloggers, and input channel allocations that were later used in the field experimental measurements. All EBTC and COTC sensors were shifted to other shields after calibration in 1998. This ensured that systematic errors did not contribute a permanent bias in any one shield.

All radiation shields were installed along an east to west transect with a separation distance of 2.43 m (Fig. 2). The height of the temperature sensor and shields for the NP were strictly set following the installation manuals. The sampling frequency of all EBTC, COTC, and NP air temperature sensors inside the ASOS, MMTS, Gill, and CRS shields was fixed at 60 s. The LI-200S pyranometer (LI-COR, Inc.) was selected to measure incoming global solar radiation (IGSR) at 1.5 m, relative to the ground surface.

3) DATA ANALYSIS

Two events were selected to illustrate the typical patterns in the EBTC model outputs. One was a clear hot day with actively growing grass covering the surface (DOY) [day of year 227, 1997]; the other was a clear cold day with snow covering the surface (DOY 70, 1998) followed by a mostly clear day with some cloudiness (DOY 71, 1998).

The SR loading was computed from Eqs. (1) to (3). The SR loading inside each shield is time- and DOY-dependent because the sun's elevation and azimuth locations are continuously changing. Therefore, we defined the SR loading ratio as 100-times solar radiation loading on the EBTC sensor inside the shield divided by the IGSR outside the shield. Only clear days were selected for our analysis of the SR ratio for each radiation shield.

An average IST for each shield provides a simple way to understand the IR contribution or IR loading because the IR incident on the temperature sensor mainly comes from the shield's inner surfaces. The average IST refers to the average of five COTC temperature readings. That is, average IST $= 0.2\,(Tc + Te + Ts + Tw + Tn)$, where Tc, Te, Ts, Tw, and Tn represent the ceiling, east, south, west, and north temperature of the shield inner surfaces, respectively. The total data points for daytime and nighttime in this analysis are 2025 and 2053 taken from DOY 15–39, DOY 121–157, and DOY 210–232, 1997.

Air temperature error is defined as the temperature difference between the NP air temperature inside the shields and the model air temperature computed from the EBTC model inside the twin shield. For the air temperature analysis, data were limited to the months of August 1997 and May 1998, when data from all sensors were available. To examine SR effects during daytime, we chose to look at the cases with high SR (IGSR above 800 W m^{-2}). For IR effects during nighttime, we examined the early morning (prior to sunrise) from local solar time 0330–0500. The resulting total number of 1-min temperature readings was 1339 for daytime effects and 1872 for nighttime effects.

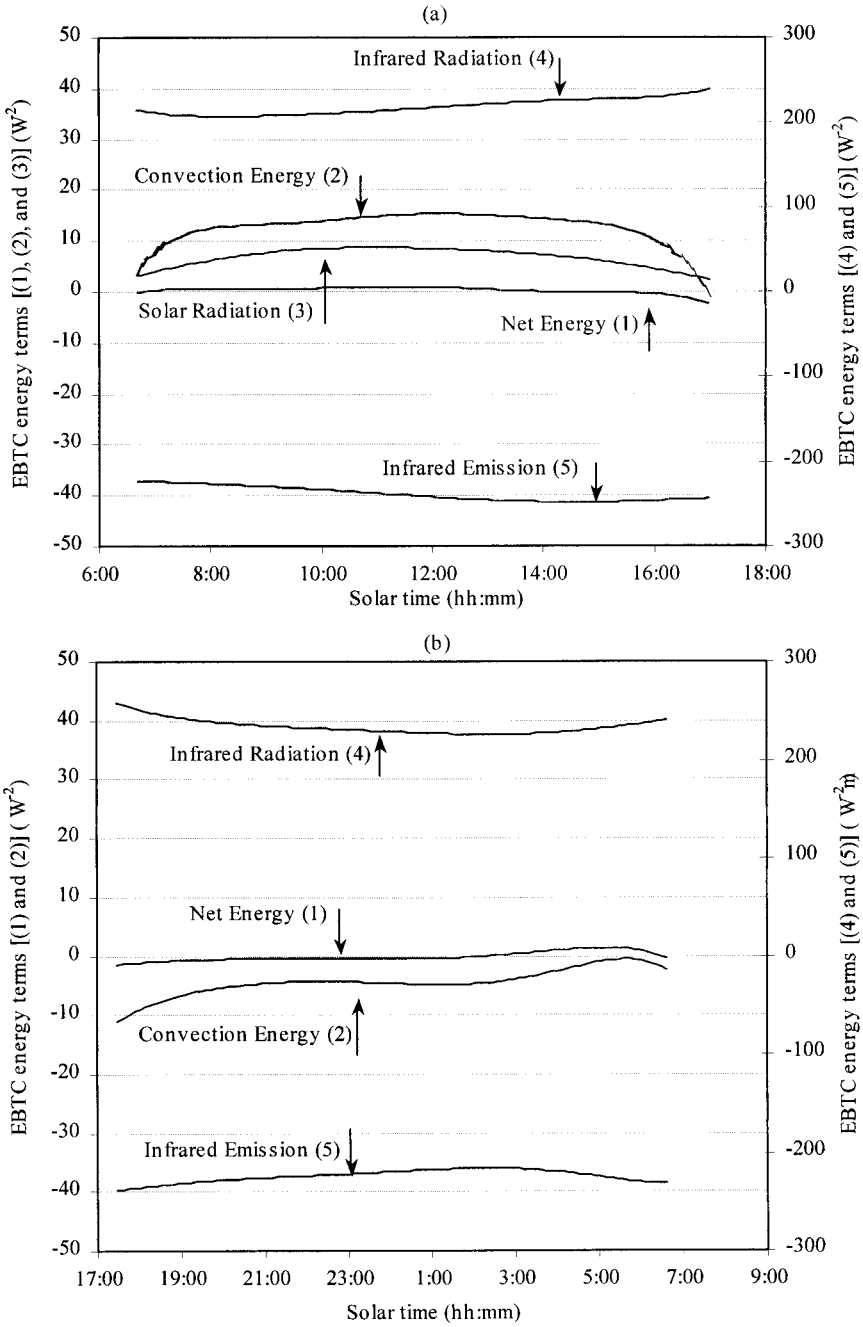

FIG. 3. The typical energy partition of a white EBTC sensor inside the CRS (DOY 70, 1998), (a) during daytime, (b) during nighttime.

3. Results

a. EBTC's energy partition patterns inside the shields

Typical daytime and nighttime values for the EBTC's energy (heat) terms [Eqs. (1)–(3)] for SR (α_{sen} SR/A), IR (ε_{sen} IR/A), convection energy [$-H(T_{sen} - T_{air})$], infrared emission ($-\sigma\varepsilon_{sen}T_{sen}^4$), and net energy [($mc\ dT_{sen}/dt$)/$A$] terms are given in Fig. 3.

Note that all energy terms were divided by the EBTC sensor area (A). The energy partitions shown are for a white EBTC sensor inside the CRS on DOY 70, 1998 and are similar to the patterns from the other radiation shields under the clear sky. Each EBTC sensor had unique energy partition patterns with terms differing in magnitude and sometimes in sign from the other EBTC sensors. These differences are the result of specific surface radiative properties of each EBTC sensor.

Under clear skies, the term α_{sen}SR/A changed with

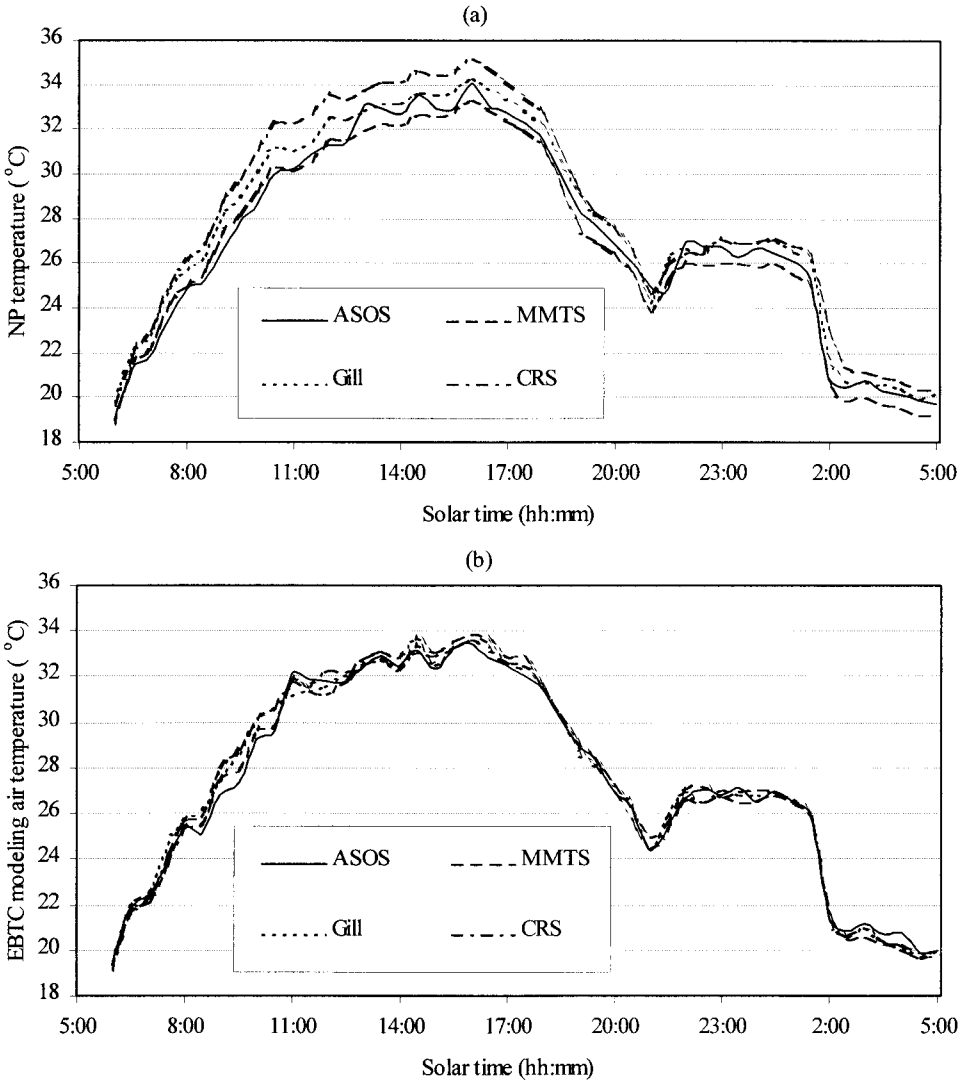

FIG. 4. (a) NP temperatures and (b) EBTC modeling air temperatures inside the shields (DOY 227, 1997).

IGSR, ground surface radiative properties, and radiation shield geometry. The SR received by the EBTC sensor inside the CRS increased during the early morning and decreased during the late afternoon (Fig. 3a). The convection energy $[-H(T_{sen} - T_{air})]$ term showed that the heat exchange was toward the sensor (positive), but the black EBTC sensor temperature was higher than air temperature, hence the convection energy term was negative.

The IR (ε_{sen}IR/A) received by the EBTC sensor was larger in magnitude than other energy terms in the EBTC model, with the exception of the infrared emission ($-\sigma\varepsilon_{sen}T_{sen}^4$) term. The infrared emission term is a function of the EBTC sensor surface temperature and its emissivity. The IR received on the surface of the EBTC sensor should be equivalent in magnitude to the infrared emission term for a good radiation shield. The net energy term should be very small because of a 1-min sampling rate and small EBTC sensor with good conductivity. It was positive when the temperature of the EBTC sensor was rising.

During nighttime, the SR (α_{sen}SR/A) term is zero. The convection energy $[-H(T_{sen} - T_{air})]$ term became smaller and the energy transfer direction was changed compared with daytime (Fig. 3b). The change in energy transfer direction occurred because the white EBTC sensor temperature during nighttime was higher than the air temperature inside the CRS. Similarly, the received IR (ε_{sen}IR/A) and infrared emission ($-\sigma\varepsilon_{sen}T_{sen}^4$) were large in magnitude.

b. Typical temperature comparison between the NP and EBTC model temperatures

Figure 4 illustrates the NP air temperatures and the EBTC model air temperatures inside the shields over

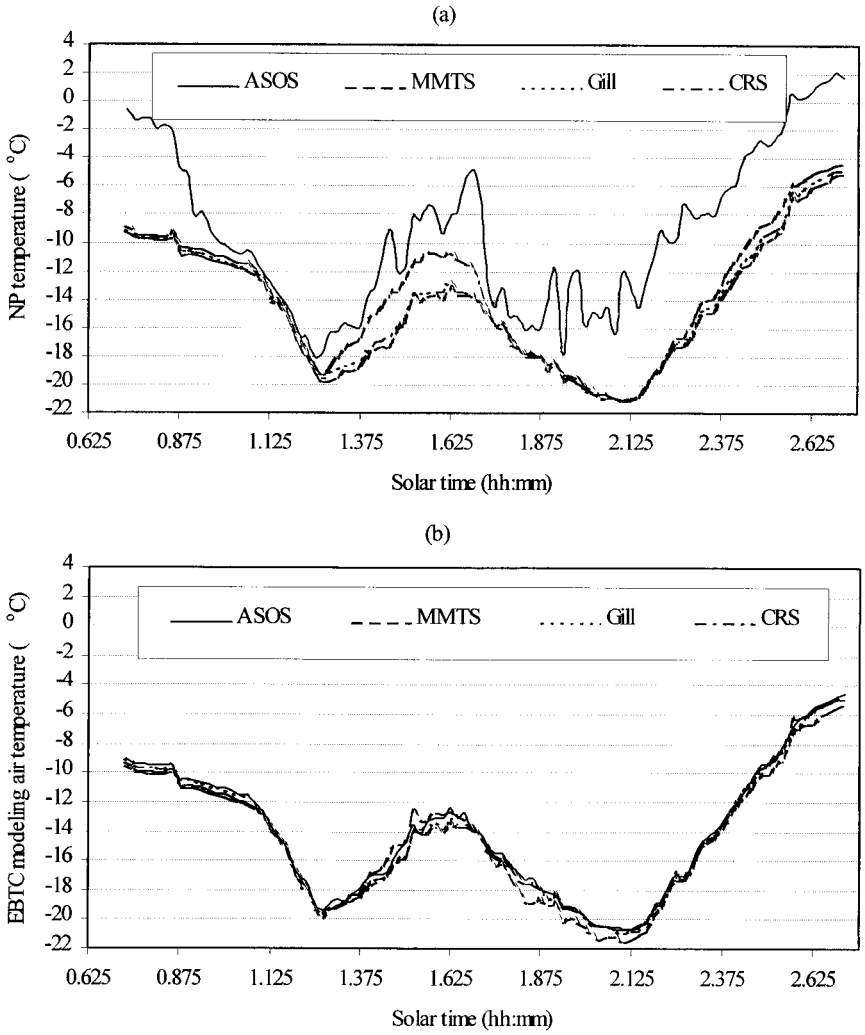

FIG. 5. Same as Fig. 4 but for DOY 69–71, 1998.

the grass surface on a clear summer day (DOY 227, 1997). The maximum NP temperature difference among the shields was about 2.3°C and the minimum was 0.36°C. The average temperature difference for the whole day was 1.38°C. However, the EBTC model air temperatures (note that the model removes the radiative and convection influences) were in good agreement from shield to shield (Fig. 4b). The maximum temperature difference among the shields was 0.97°C and minimum was 0.016°C. The average temperature for the whole day was 0.34°C. Among the NP temperatures, the CRS temperatures were highest, the Gill temperatures were next highest, and the ASOS and MMTS were the lowest. The temperature differences among all shields were increasingly larger from sunrise to sunset. However, the difference during small IGSR and nighttime were obviously smaller. The difference between Figs. 4a and 4b reveals that each shield has its own microclimate environment in the limited space of the radiation shields, and for this reason the NP temperatures ''sensed'' are biased accordingly.

Comparison of NP air temperatures among the shields during cold and snow cover conditions revealed poor performance (Fig. 5a), especially for ASOS. The EBTC model temperatures were again in close agreement (Fig. 5b). The ASOS's NP air temperature was systematically affected during both daytime and nighttime for this case. Thus, the ASOS anomalies (Fig. 5a) could not be attributed to solar radiative heating or cooling effects. The average temperature difference for these two days was 5.2°C but only 0.48°C for the EBTC model air temperatures.

c. SR loading of the EBTC sensor inside the shields

The average SR loading ratio provided a means to evaluate the solar shielding effectiveness of a temperature radiation shield. Figure 6 shows how the average

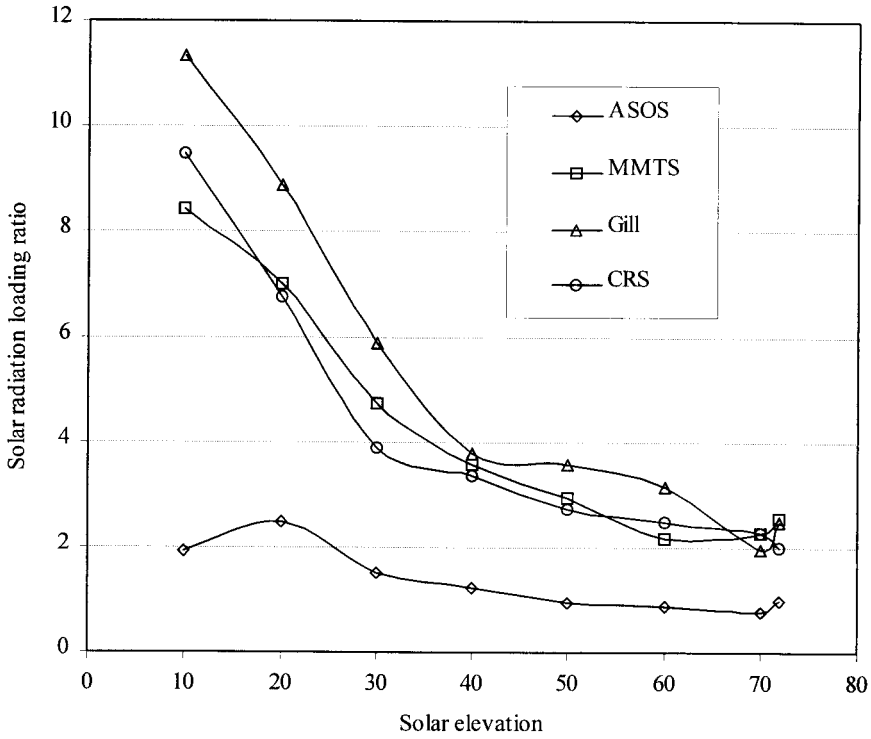

FIG. 6. SR loading ratio inside the shields. Each point represents the averaging value of 1° of solar elevation angle. Maximum solar elevation in Lincoln, NE, is 73°.

SR ratio changes with solar elevation. The maximum solar elevation angle reached at our experiment site is 73°. With respect to SR shielding effectiveness, the Gill shield performance was the poorest of the four shields. The ASOS had optimal SR shielding. Both MMTS and CRS shields were rated between the Gill and ASOS shields, but their trends are very similar to the Gill shield. Therefore, the interior SR loading ranked as

$$\text{Gill} > \text{MMTS} \approx \text{CRS} > \text{ASOS}.$$

d. IR loadings and IST

Due to the large magnitudes of IR terms in Eqs. (1)–(3) (Fig. 3), the IR values among shields overlapped, making it difficult to extract differences (sensible signals) even for the long-term average computations. For this reason, the difference between the shield average IST and average NP sensor temperature was taken as an indicator to evaluate the IR loading for each shield. During daytime, the distribution of temperature differences for all shields demonstrated similar Gaussian shapes, with the modes around −0.5°, −0.5°, 0°, and 1°C, respectively, for the Gill, MMTS, CRS, and ASOS shields (Fig. 7). However, the mean values of each shield were −0.55°, −0.26°, +0.01°, and +0.88°C, respectively, for the Gill, MMTS, CRS, and ASOS shields. Unexpectedly the Gill and MMTS shields had negative means for temperature difference values. This statistical result contradicts findings in previous literature (McTaggart-Cowan and McKay 1976; McKay and McTaggart-Cowan 1977; Tanner et al. 1996), which reported that the radiation shields IR) might heat the air or air temperature sensor inside the shields during daytime. For our measurements, the magnitude of average temperature difference between the shield IST and sensor temperature during the daytime ranked as

$$\text{ASOS} > \text{Gill} > \text{MMTS} \geq \text{CRS}.$$

During nighttime, the modes of shield temperature difference distributions were approximately zero (Fig. 7b). But the average values were −0.20°, −0.12°, −0.07°, and −0.20°C for the ASOS, MMTS, Gill, and CRS shields, respectively. Previous literature stated that shield temperature might be cooler than sensor temperature during nighttime. However, in this study heating and cooling effects on the sensors were uniformly distributed around zero during nighttime. Only the ASOS shield distribution was slightly skewed toward cooling effects.

e. NP air temperature errors caused by radiative effects

Both SR and IR can cause radiative heating errors to the NP air temperature during daytime, while the IR may or may not cause underestimation of NP air temperature, depending on radiative exchanges between sensor surface and shield inner surface. Figure 8 shows the NP air temperature errors associated with the am-

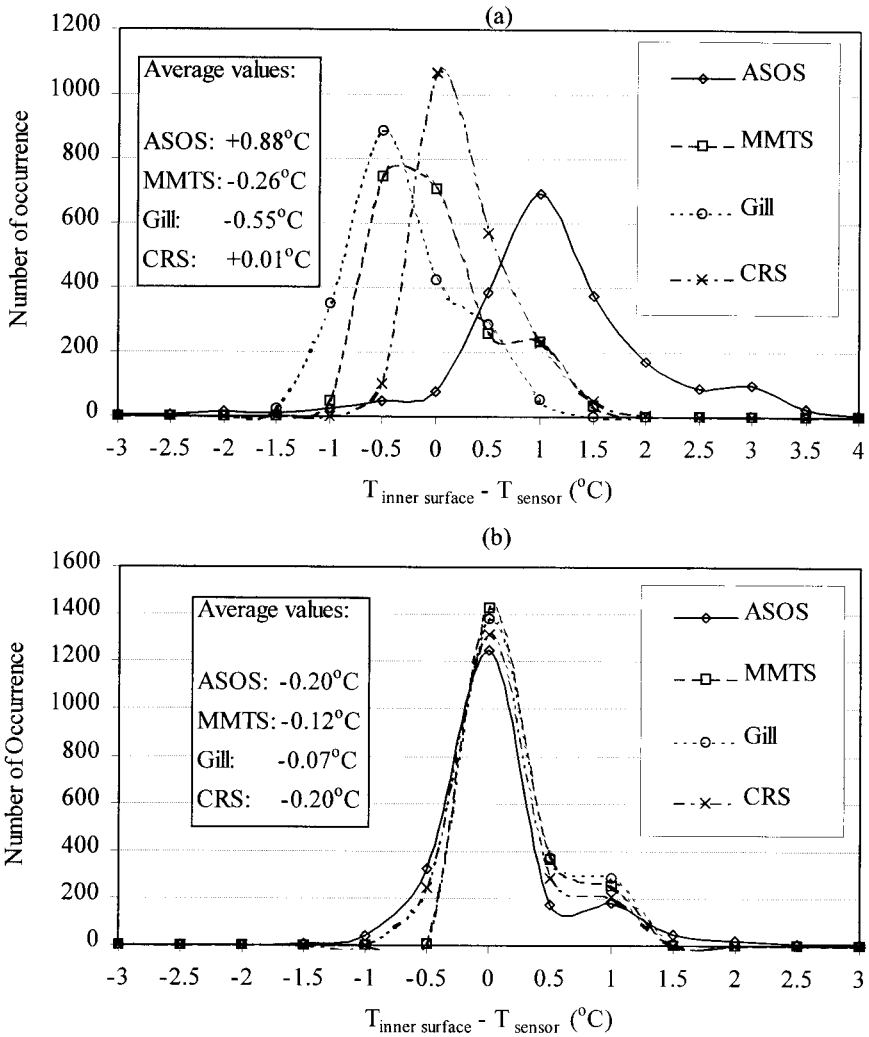

FIG. 7. Temperature differences between the average IST of shield and sensor temperature inside the shield during (a) daytime and (b) nighttime.

bient wind speed. Daytime data were limited to ambient wind speeds greater than 1 m s^{-1} because of the variability and possible bias associated with anemometer start-up speed. Air temperature errors were analyzed according to wind speed interval (1 m s^{-1}). The error bars represent 1.96 times the standard deviation (i.e., 95% confidence interval). The trends in air temperature error as a function of ambient wind speed indicate that errors from radiative heating effects decreased with increasing ambient wind speed. Due to different systematic biases inherent in each NP temperature system, it is not possible to generalize at this point or state which NP air temperature system was more susceptible to high SR at a given wind speed. Under high SR conditions, all NP air temperature systems except the ASOS were strongly affected by ambient wind speed and therefore not able to measure air temperature with the accuracy claimed by NP temperature sensor manufacturers. The aspirated ASOS is believed to be independent of the ambient wind speed; however, under low ambient wind speed the IR effects from the ASOS's shield surface may be accelerated.

Similarly, the average NP air temperature errors were affected by the IR (Fig. 9). The data points and error bars in Fig. 9 have the same meanings as those in Fig. 8. At this time of day, no apparent effects or trends were due to the ambient wind speed. However, the variations in the NP air temperature at the low ambient wind speed were larger and equally scattered about zero. The variations in the NP air temperature errors became smaller as the wind speed increased.

Large variations in errors were observed at low ambient wind speed for daytime and nighttime (Figs. 8 and 9). In addition to the sources of noise in the EBTC system, another possible explanation is that each NP air temperature system has its own thermal time constant (thermal lag). The sensor time constant and radiation shield time constant are different, and thus, the shield

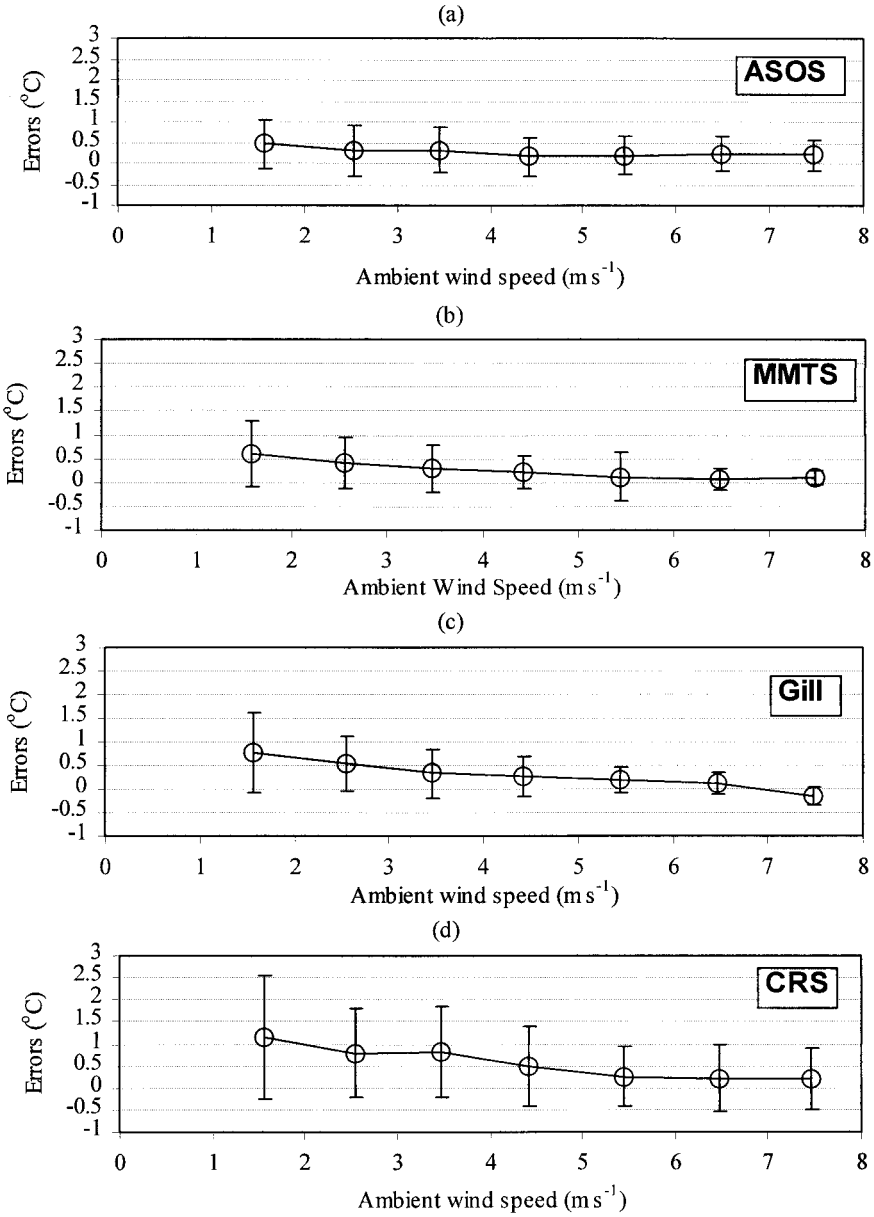

FIG. 8. NP air temperature errors for (a) the ASOS system, (b) the MMTS system with CR10 datalogger, (c) the Gill shield with an HMP35C sensor, and (d) the CRS shield with an HMP35C sensor for incoming global SR above 800 W m^{-2} and ambient wind speed of 3 m.

temperature changes are not synchronous with the temperature sensor changes.

4. Discussion and conclusions

The EBTC model [Eqs. (1)–(3)] suggests that an ideal air temperature shield should remove both SR (SR = 0) and net IR (IR $- A\sigma T_{\text{sen}}^4 = 0$) effects on the air temperature sensor while minimizing the blockage of air flow. In addition, the conduction energy effects, including the thermal conduction and electrical conduction, should be zero. If the convection heat transfer coefficient H in the convection heat transfer term $[-AH(T_{\text{air}} - T_{\text{sen}})]$ is sufficiently large, it will improve the ability of T_{sen} to represent T_{air}. In other words, an increase in the airflow speed inside the shield will enhance the degree to which temperature sensor readings inside the shield represent the air temperature. The naturally ventilated shields used in this study did not satisfy this requirement under light wind conditions. Aspirated shields with minimal electrical-motor heat generation away from the temperature sensor are preferable for future weather station networks.

The EBTC model offers a means of measuring the

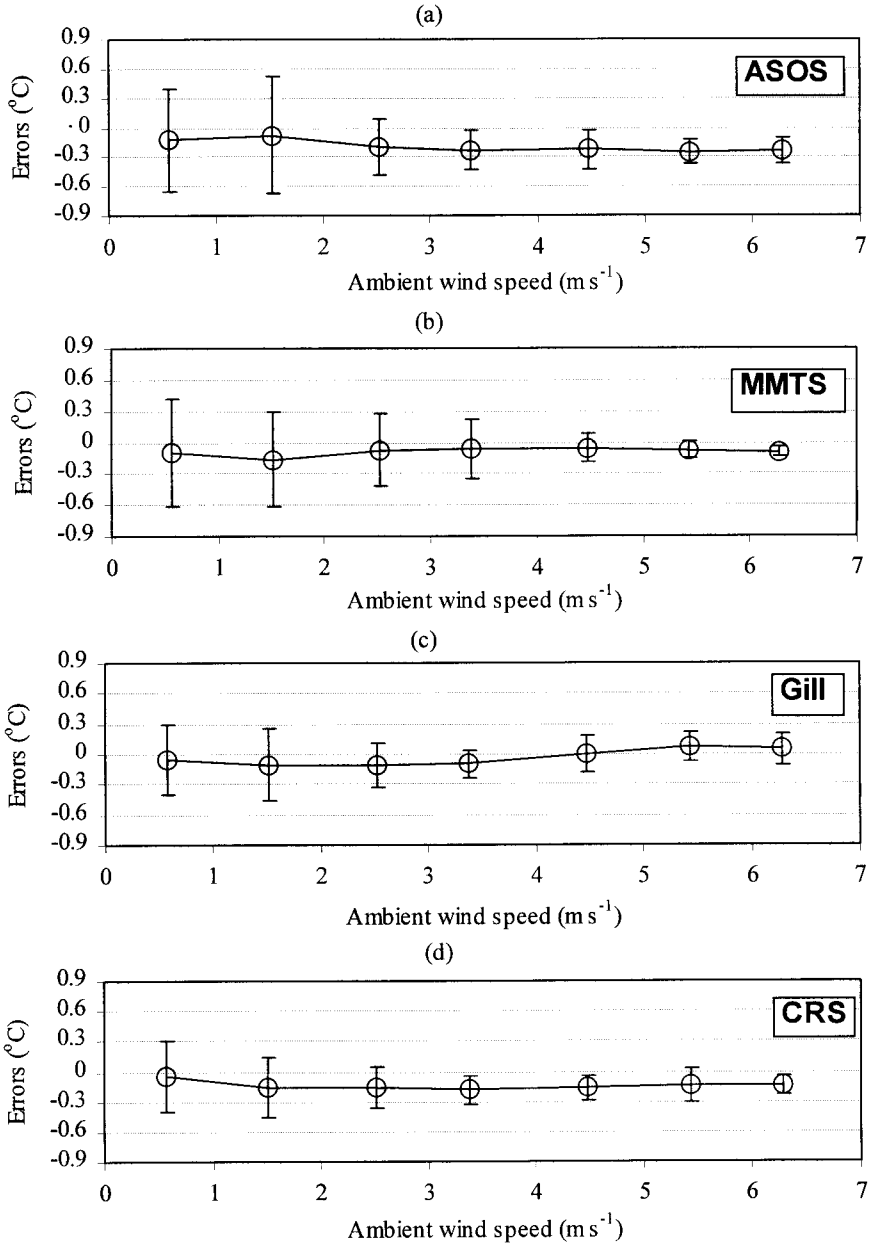

FIG. 9. The normal operating (NP) air temperature errors for (a) the ASOS system, (b) the MMTS system with CR10 datalogger, (c) the Gill shield with an HMP35C sensor, and (d) the CRS shield with an HMP35C sensor during early morning from solar time 0300 to 0430 for ambient wind speed at 3 m.

real-time air temperature (Figs. 4 and 5) while simultaneously removing the SR and IR effects inside the shields. The accuracy of the EBTC model is related to the EBTC design and the accuracy of model parameters. According to Luers (1992), the absolute accuracy of the EBTC model can reach better than ± 0.3°C if the accuracy of the EBTC sensor temperature is better than ± 0.2°C, the emissivity and absorptivity measurement error is within ± 0.05, and the conduction of heat through extension wires and sensor supports is sufficiently small.

The SR loading ratio inside the shields indicated in Fig. 6 reflects the SR distribution at the NP air temperature sensor position during the daytime under clear days. The interior SR ratios for all shields rank as follows:

$$\text{Gill} > \text{MMTS} \approx \text{CRS} > \text{ASOS}.$$

Based on the magnitude of average temperature difference between shield inner surface and sensor temperature, the IR effects on air temperature measurements rank as follows:

$$\text{ASOS} > \text{Gill} > \text{MMTS} > \text{CRS}$$

during daytime. Both MMTS and Gill shields showed the cooling effects due to shield temperature in terms of their average values. During nighttime, the infrared effects were smaller. On average, the nighttime infrared effects could be considered negligible for all shields except the ASOS shield, which had a slight cooling effect (Fig. 7). Therefore, we conclude that the ASOS infrared shielding performance was poorest among the tested shields.

Normal operating air temperature errors caused by radiative effects during daytime and nighttime (Figs. 8 and 9) are consistent with the work of Gill (1983) and Tanner et al. (1996), who demonstrated the radiation shield performance on the sensor temperature. The radiative effect on the air temperature errors at nighttime should be a minor influence (Figs. 7b and 9), but it did exist (McTaggart-Cowan and McKay 1976; McKay and McTaggart-Cowan 1977; Tanner et al. 1996) and caused either heating or cooling, especially under the lower ambient wind speed. The NP air temperature errors (Figs. 8 and 9) cannot be considered solely as the radiation effect or air flow effects because NP air temperature sensors likely do not have a non-zero-systematic bias in this case. The SR and IR effects can degrade the accuracy of NP temperatures, especially when the ambient wind speed is low (e.g., <4 to 5 m s^{-1}). The NP air temperature errors inside the shield are related to accuracy of the temperature sensor, the use of extension wire, and accuracy of the data acquisition system (as in the performance of electronic components, accuracy of the software algorithm, and external random interferences; Valvano 1992).

A possible transfer function is suggested:

$$T_{\text{NP}} - T_{\text{air}} = E_{\max} f(\text{IGSR, wind speed, albedo}) + \delta_{\text{NP}}, \quad (8)$$

where T_{NP} represents the NP temperature readings inside the specific radiation shield; $E_{\max}$ represents the maximum error caused by the IGSR, ambient wind speed, and surface albedo under extreme conditions; f represents a function; and δ_{NP} represents the statistically systematic bias of the NP air temperature sensor, which includes both sensor error and data acquisition error. An improved EBTC model to give a true measure of ''air temperature'' is needed to reveal the form of the air temperature correction model of Eq. (8).

The feasibility of correcting air temperature errors due to the radiation shield microclimate has been demonstrated but will require more investigation before a transfer function [e.g., Eq. (8)] for each specific shield can be developed. This study indicates that the essential parameters in a correction model include the real-time IGSR, real-time ambient wind speed, and the empirical ground surface albedo value at the weather station site. Air temperature corrections to the ASOS, MMTS, Gill, and CRS measurements may be attainable. We plan to continue this research by further comparing normal operation systems with an improved EBTC system.

Acknowledgments. This research was supported by a National Weather Service fellowship program and the High Plains Regional Climate Center at the University of Nebraska at Lincoln. The authors wish to thank Drs. David Jones and Qi ''Steve'' Hu for the valuable comments and discussion on the original manuscript.

REFERENCES

Andresen, J. A., and F. V. Nurnberger, 1997: A field comparison of operational temperature sensors. Preprints, *10th Conf. on Applied Climatology,* Reno, NV, Amer. Meteor. Soc., 157–160.

ASOS Program Office, 1992: Automated surface observing system site technical manual S100. AAI Systems Management Incorporated.

Blackburn, T. M., 1993: Effects on climate change resulting from changes in National Weather Service cooperative station instrumentation and siting conditions. Preprints, *Eighth Symp. on Meteorological Observations and Instrumentation,* Anaheim, CA, Amer. Meteor. Soc., J6–J11.

Bradley, J. F., 1994: Interim results of the climatic temperature study. U.S. Department of Commerce Misc. Rep., NOAA/NWS Test and Evaluation Division, 20 pp.

Bradley, J. T., and J. F. Bradley, 1995: CRS-MMTS temperature comparison study. U.S. Department of Commerce Misc. Rep., NOAA/NWS Test and Evaluation Division, 20 pp.

Brock, F. V., J. Richardson, and S. R. Semmer, 1995a: Passive multiplate solar radiation shields. Preprints, *Ninth Symp. on Meteorological Observations and Instrumentation,* Charlotte, NC, Amer. Meteor. Soc., 329–334.

——, S. R. Semmer, and C. Jirak, 1995b: Passive solar radiation shields: Wind tunnel testing. Preprints, *Ninth Symp. on Meteorological Observations and Instrumentation,* Charlotte, NC, Amer. Meteor. Soc., 179–183.

Canfield, N. L., and J. A. McNitt, 1991: Automated Surface Observing System data for climatic analysis, research and service. Preprints, *Seventh Symp. on Meteorological Observations and Instrumentation,* New Orleans, LA, Amer. Meteor. Soc., 213–216.

Croft, P. J., and D. A. Robinson, 1993: The impact of MMTS on the New Brunswick climate record. Preprints, *Eighth Symp. on Meteorological Observations and Instrumentation,* Anaheim, CA Amer. Meteor. Soc., J12–J15.

Dewitt, D. P., and G. D. Nutter, 1989: *Theory and Practice of Radiation Thermometry.* Wiley Interscience, 1138 pp.

Doesken, N. J., T. B. McKee, and J. W. Harrington, 1995: MMTS—Ten years after. Preprints, *Ninth Symp. Conf. on Applied Climatology,* Dallas, TX, Amer. Meteor. Soc., 21–24.

Easterling, D. R., R. G. Quayle, and P. Y. Hughes, 1993: The effects of thermometer changes on the temperature record of U.S. first-order stations. Preprints, *Eighth Symp. on Meteorological Observations and Instrumentation,* Anaheim, CA, Amer. Meteor. Soc., J3–J5.

Fuchs, M., and C. B. Tanner, 1965: Radiation shields for air temperature thermometers. *J. Appl. Meteor.,* **4,** 544–547.

Gall, R., K. Young, R. Schotland, and J. Schmit, 1992: The recent maximum temperature anomalies in Tucson: Are they real or an instrument problem? *J. Climate,* **5,** 657–665.

Gill, G. C., 1979: Development of a small radiation shield for air

temperature measurements on drifting buoys. NOAA Buoy Office Rep., Contract 01-7-038-827, 23 pp.
——, 1983: Comparison testing of selected naturally ventilated solar radiation shields. NOAA Buoy Office Rep., Contract NA-82-0A-A-266, 15 pp.
Guttman, N. B., and C. B. Baker, 1996: Exploratory analysis of the difference between temperature observations recorded by ASOS and conventional methods. *Bull. Amer. Meteor. Soc.*, **77,** 2865–2873.
Holman, J. P., 1997: *Heat Transfer*. 8th ed., McGraw-Hill, 696 pp.
Karl, T. R., J. D. Tarpley, R. G. Quayle, H. F. Diaz, D. A. Robinson, and R. S. Bradley, 1989: The recent climate record: What it can and cannot tell us. *Rev. Geophys.*, **27,** 405–430.
Kessler, R. W., L. F. Bosart, and J. Kleist, 1993: Recent maximum temperature anomalies at Albany, New York: Fact or fiction? *Bull. Amer. Meteor. Soc.*, **74,** 215–226.
Lin, X., 1999: Microclimate inside air temperature radiation shields. Ph.D. thesis, University of Nebraska, Lincoln, 187 pp.
——, K. G. Hubbard, and G. E. Meyer, 2001: Airflow characteristics of commonly used temperature radiation shields. *J. Atmos. Oceanic Technol.*, **18,** 329–339.
Luers, J. K., 1989: The influence of environmental factors on the temperature of the radiosonde thermistor. Ph.D. thesis, University of Tennessee, 169 pp.
——, 1992: Absolute accuracy of the multi-thermistor radiosonde for measuring atmospheric temperature. NASA Goddard Space Flight Center Rep., Contract NAS5-31661, 54 pp.
——, and R. E. Eskridge, 1995: Temperature corrections for the VIZ and Vaisala radiosondes, *J. Appl. Meteor.*, **34,** 1241–1253.
MacHattie, L. B, 1965: Radiation screens for air temperature measurements. *Ecology*, **46,** 533–538.
McKay, D. J., and J. D. McTaggart-Cowan, 1977: An intercomparison of radiation shields for auto stations. *WMO Tech. Conf. on Instruments and Methods of Observation*, Geneva, Switzerland, WMO No. 480, 208–213.
McKee, T. B., N. J. Doesken, and J. Kleist, 1993: A preview of temperature and precipitation data continuity into the ASOS (Automated Surface Observing System) era. Preprints, *Eighth Symp. on Meteorological Observations and Instrumentation*, Anaheim, CA, Amer. Meteor. Soc., J16–J21.
McTaggart-Cowan, J. D., and D. J. McKay, 1976: Radiation shields—An intercomparison. Atmospheric Environment Service of Canada Misc. Rep., 9 pp.
Meyer, S. J., and K. G. Hubbard, 1992: Nonfederal automated weather stations and networks in the United States and Canada: A preliminary survey. *Bull. Amer. Meteor. Soc.*, **73,** 449–457.
National Weather Service, 1983: Maximum/minimum temperature system operation instructions. NWS Misc. Rep., 5 pp.
OMEGA Engineering, Inc., 1995: *The Temperature Handbook*. Vol. 29. OMEGA Engineering, Inc., Stamford, CT, 1494 pp.
Quayle, R. G., D. R. Easterling, T. R. Karl, and P. Y. Hughes, 1991: Effects of recent thermometer changes in the cooperative station network. *Bull. Amer. Meteor. Soc.*, **72,** 1718–1723.
Richardson, S. J., and F. V. Brock, 1995: Passive solar radiation shields: Energy budget—Optimizing shield design. Preprints, *Ninth Symp. on Meteorological Observations and Instrumentation*, Charlotte, NC, Amer. Meteor. Soc., 259–264.
Robinson, D. A., 1990: The United States cooperative climate-observing system: Reflections and recommendations. *Bull. Amer. Meteor. Soc.*, **71,** 215–226.
Schmidlin, F. J., H. Sang Lee, and B. Ranganayakamma, 1995: Deriving the accuracy of different radiosonde types using the three-thermistor radiosonde technique. Preprints, *Ninth Symp. on Meteorological Observations Instrumentation*, Charlotte, NC, Amer. Meteor. Soc., 27–31.
Sterling Research & Development Center, 1973: Test and evaluation of the Israeli instrument shelter. Lab. Interim Rep. 8/73, National Weather Service Functional Experimentation and Testing Branch, 14 pp.
Tanner, B. D., E. Swiatek, and C. Maughan, 1996: Field comparisons of naturally ventilated and aspirated radiation shields for weather station air temperature measurements. Preprints, *22d Conf. on Agricultural and Forest Meteorology*, Atlanta, GA, Amer. Meteor. Soc., 227–230.
Tarnopolsky, M., and I. Seginer, 1999: Leaf temperature error from heat conduction along thermocouple wires. *Agric. For. Meteor.*, **9,** 185–194.
Valvano, J. W., 1992: Temperature measurements. *Advances in Heat Transfer. Bioengineering Heat Transfer*, Y. I. Cho, Ed., Book News, 359–436.
Wendland, W. M., and W. Armstrong, 1993: Comparison of maximum-minimum resistance and liquid-in-glass thermometer records. *J. Atmos. Oceanic Technol.*, **10,** 233–237.
Whitaker, S., 1972: Forced convection heat-transfer corrections for flow in pipes, past flat plates, single cylinders, single sphere, and flow in packed bids and tube baundles. *AIChE J.*, **18,** 361–371.
Wylie, R. G., and T. Lalas, 1992: Measurement of temperature and humidity: Specification, construction, properties and use of the WMO reference psychrometer. WMO Rep. 759, 71 pp.